Journal of Building Engineering 82 (2024) 108344

Contents lists available at ScienceDirect

Journal of Building Engineering

journal homepage: www.elsevier.com/locate/jobe

Coupling effect of radiative cooling and phase change material on building wall thermal performance

Zhaoli Zhang [a], Jiayu Liu [a], Nan Zhang [a,*], Xiaoling Cao [a], Yanping Yuan [a,b], Muhammad Sultan [c], Shady Attia [d]

[a] School of Mechanical Engineering, Southwest Jiaotong University, Chengdu 610031, China
[b] School of Civil Engineering and Architecture, Chongqing University of Science and Technology, Chongqing 401331, China
[c] Department of Agricultural Engineering, Bahauddin Zakariya University, Multan 60800, Pakistan
[d] Sustainable Building Design Lab, Dept. UEE, Faculty of Applied Sciences, University of Liège, Liège 4000, Belgium

ARTICLE INFO

Keywords:
Radiative cooling
Phase change material
Coupling effect
Multilayer wall
Building energy conservation

ABSTRACT

Phase change material (PCM) featured with high latent heat thermal energy storage capacity and isothermal phase transition is employed into building walls decorated with radiative cooling (RC) coating, in order to modify the cooling effect on building thermal performance. Numerical analysis indicates that the RC coating causes exterior temperature of P-RC walls lower than ambient temperature, achieving maximum exterior temperature drop of 13.63 °C. Thermal buffer effect of PCM enables to shave the temperature peak and shift the temperature valley, inducing exterior temperature of the P-RC wall to fluctuate slightly in comparison to the RC wall. Interior temperature of the P-RC wall is found to approach to target temperature tightly. PCM located closer to the outside completes phase transition more rapidly, which is beneficial to levelling radiative cooling of RC coating. Exterior temperature of P-RC walls increases with augment of solar radiation intensity, ambient temperature and indoor temperature. Augment of PCM thickness, ambient temperature or indoor temperature is conducive to interior temperature. Latent heat thermal energy storage of PCM enlarges effective thermal capacity of walls, which is favorable to maintain interior temperature within target temperature. In conclusion, studied results highlight that radiation cooling can be improved by PCM, with substantial benefits to develop passive cooling available to building energy conservation.

1. Introduction

Building cooling has become a critical energy concern during the process to build indoor thermal comfortable environment, approximately accounting for 30 % of the total final energy utilization [1,2]. Mechanical compression refrigeration system is the mainstream form of air-conditioning systems with the consumption of electricity [3]. Carbon dioxide is inevitably released during the power production from fossil fuels, which leads to environmental pollution and energy crisis. Passive radiative cooling is discovered as an attractive approach to deal with the building cooling, by means of providing a perpetual path to dissipate heat without energy consumption [4,5].

The Earth atmosphere has a highly transparent window in the infrared wavelength range between 8 and 13 μm that is known as the atmospheric window [6,7]. Coincidentally, the atmospheric window falls within the peak thermal radiation of a black body defined by

* Corresponding author.
E-mail address: zhangn09@swjtu.edu.cn (N. Zhang).

https://doi.org/10.1016/j.jobe.2023.108344
Received 13 September 2023; Received in revised form 5 December 2023; Accepted 15 December 2023
Available online 16 December 2023

Plank law at the ambient temperature (27 °C), producing passive cooling for a terrestrial object by eliminating heat via radiative emission through the atmospheric window [8]. Radiative cooling is based on the principle of long-wave radiation emission from a high temperature object to a lower one [9–11]. Considering temperature of the ultracold universe can drop down to 3 K, it is termed as a natural heat sink to building cooling, which offers a cooling power of more than 100 W/m^2 under optimized device designs and suitable atmospheric conditions [12]. Majority of earth radiation can be radiated from the atmospheric window to outer space, achieving positive cooling effect on buildings [13]. Earlier usage of radiative cooling comprising infrared emission is mainly conducted at nighttime.

Khedari et al. [14] discussed feasibility of cooling by using night radiation under Thailand hot and humid climate. The depression of different surface temperatures was 1–6 °C below ambient temperature under clear and cloudy skies. Factors affecting night radiation cooling were sky conditions, thermal emissivity of materials and water condensation on the radiator surface. Meir et al. [15] designed a radiative cooling system consisting of unglazed flat plate radiators, water as heat carrier and a reservoir. Impact of the tilt angle, the aperture area and the reservoir volume on cooling performance were studied under Oslo climate. Radiative cooling system enabled to cover the demand, except for mid-summer ambient temperature and high relative humidity. Heidarinejad et al. [16] presented results of a hybrid system consisting of nocturnal radiative cooling, cooling coil, and direct evaporative cooling in Tehran. Overall effectiveness of the hybrid system was more than 100 %, indicating that this environmentally clean and energy efficient system could be considered as an alternative to the mechanical vapor compression system. Zhang et al. [17] combined a MPCM slurry storage with a nocturnal radiative cooling system to analyze cooling energy consumption and energy-free nocturnal radiation. Energy saving potential in Lanzhou and Urumqi could reach 77 % and 62 % for low-rise buildings. The hybrid system was recommended to be used in northern and central China. Tso et al. [18] analyzed radiative cooling under Hong Kong hot and humid climate. The passive radiative cooler with seven KCl windows provided a satisfactory cooling effect at night, with the ambient air temperature reduced by about 6–7 °C. Cooling capacity of the passive radiative cooler without vacuum achieved 38 W/m^2 under a clear night sky. Sameti et al. [19] studied solar passive heating and radiative cooling for a building. The space was passively cooled via natural convection from surface of the storage subsystem with a storage tank pre-cooled by night sky radiation. The optimized transparent layer absorptivity, parametric sensitivity and temperature profiles were illustrated in their investigation.

Cooling ability of radiators lies in the radiative emission profiles. The radiation escapes to the outer space through the Earth atmosphere. An ideal emitter should selectively and strongly emit (emissivity>90 %) in the atmospheric window [20]. Theoretically, the atmospheric window allows outgoing radiative emission of a terrestrial object to exceed its absorbed incoming atmospheric radiation at night, resulting in temperature lower than the ambient (sub-ambient effect). Previous studies testify that these conventional radiative coolers enable to dissipate thermal energy from buildings that is beneficial to create thermal comfortable environment at nighttime [21,22]. However, cooling performance of a radiative cooler is dependent on many factors, such as the incoming atmospheric radiation, the nonradiative (conductive and convective) heat gain from the surrounding media and the incoming solar radiation during the daytime. The incoming solar radiation during the daytime will become strong in summer or in tropic region. Cooling capacity of a radiative cooler reduces as growth of incoming solar radiation, hardly achieving sub-ambient effect at daytime when incoming solar radiation exceeds its outgoing radiation [23]. Recent progress reports novel radiative coolers to realize efficient cooling and ability to operate directly under the sun, gaining daytime temperature below the ambient temperature as well. Numerous pioneer studies towards applications of the improved radiative coolers have been carried out.

Wang et al. [24] measured the indoor air temperature, roof temperature and building cooling energy consumption of a commercial warehouse covered a scalable-manufactured radiative cooling metamaterial film. Annual cooling energy saving of the built warehouse could reach 65.2 % over the baseline. Cheng et al. [25] proposed a biomimetic wrinkle structure combined with optimized particles to achieve the efficient optical property regulation to both the solar band and atmospheric window band. Maximum average indoor air temperature painted with the coating was reduced by 6.2 °C with maximum power saving rate of air conditioning exceeding 50 %. Yi et al. [26] designed a transparent radiative cooling film with low transmittance in solar spectra and selectively high emissivity in the atmospheric window on roof glazing of buildings. Annual air conditioning energy consumption of the building could reduce by 40.9%–63.4 %. Zhou et al. [27] developed a detailed model-based framework for system-level integration of water-based daytime radiative cooling panels with heat exchangers and cold storage to cool the residential building. Optimal water flow rate contributed to air temperature reduction of approaching 12.7 °C for a typical single-family house in the U.S. Anand et al. [28] assessed improvements in each rooftop radiative property impacting on surface temperatures and heat fluxes. Rooftop materials with solar reflectance above 0.9 resulted in surface temperatures always below ambient and cooling power of more than 30 W/m^2 during summer. Yoon et al. [29] configured a hybrid heating, ventilation, and air-conditioning system coupled with a solar thermal collector and a radiative cooling panel as a heat source and a heat sink. The proposed system was found to be able to reduce the annual power consumption by about 3%–29 %, compared to the conventional system. Lin et al. [30] prepared a flexible and scalable daytime passive radiative cooler consisting of a reflector layer and a polydimethylsiloxane layer to achieve sub-ambient cooling in Hong Kong hot and humid climate. Cooling powers of 52.4 W/m^2 and 84.7 W/m^2 were measured at noon and night under clear sky condition. The daytime passive radiative cooling could be potentially applied in buildings and vehicles. Tang et al. [31] evaluated thermal regulation from an all-season perspective by preparing a mechanically flexible coating that adapts its thermal emittance to various ambient temperatures. The fabricated temperature-adaptive radiative coating absorbed solar energy and switched thermal emittance from 0.20 for temperatures below 15 °C to 0.90 for temperatures above 30 °C, driven by a photonically amplified metal-insulator transition.

Based on the above reviews, radiative cooling exerts a vital impact on practical building energy saving applications with its highly efficient passive cooling [9]. The incoming solar radiation dominated by the solar reflectance has significant effect on diurnal radiative cooling. A highly emissive radiator possessing high solar reflectance enables to deliver passive cooling during the daytime, leading to temperatures well below the ambient [27]. Radiative emission and solar reflection can be adjusted via polymers (PMMA, PDMS, PVF),

inorganic particles or films (silicon monoxide, silicon dioxide, silicon oxynitride) and wood nanofibers. However, the practical realization of novel radiative radiators is still a serious challenge. Continuing cooling of radiative radiators not only achieve building cooling, but also may lead to supercooling at low ambient temperature condition, increasing the heating demand accordingly [32]. Intelligent materials subjected to thermochromism, electrochromism and mechanical response are emerging methods for regulation mode switching. They enable to modulate transmittance over the solar wavelength range to realize the dynamic switch between a strong and a weak heating regulation mode [26,30,31]. Whereas, dynamic tuning requires external energy input and continuous operational maintenance, resulting in decreased lifetime and increased levelized cost of energy. Phase Change Material (PCM) refers to a substance that absorbs or releases thermal energy through its phase transition, which can potentially work as a thermal buffer to supercooling [33–35]. In most cases, the energy storage related phase transition will occur between solid and liquid states. PCM is capable of storing or releasing amounts of thermal energy under almost isothermal condition [36–38]. When incorporated into the buildings, PCM theoretically endows building envelopes to have enhanced thermal capacity, which is conduce to eliminating supercooling caused by radiative cooling, maintaining indoor thermal comfortable environment for occupants. Effect of ambient temperature variation on building thermal performance can also be degraded via PCM incorporation.

Cooling of a radiative cooler and thermal energy storage of PCM jointly guarantee indoor thermal comfortable environment at higher ambient temperature. PCM enables to improve thermal capacity of building walls, which is expected to modify the radiation cooling effect on wall thermal performance. This study aims to evaluate the coupling effect of radiative coating and PCM when simultaneously integrated into the building walls. A reliable numerical model is initially developed to investigate heat transfer process of a building wall containing a radiative cooler and a PCM layer. This study assesses the influence of PCM addition, location and thickness on wall thermal performance. Several factors (solar radiation, ambient temperature and indoor temperature) are also included in the parametric analysis.

2. Numerical investigation

2.1. Physical model

An office in the multistory building with the south wall receiving solar radiation is selected in this study. Detailed configuration of the south wall is illustrated in Fig. 1(b). It is observed that the south wall mainly consists of five layers materials. The building materials from the inside out are respectively interior mortar, concrete, PCM, exterior mortar and RC coating. The innermost side refers to decorative mortar (20 mm) that connects with indoor environment directly. 200 mm concrete is arranged on outside of the mortar in order to provide structural support of the wall. A PCM layer with variable thickness of 20–50 mm is placed between the concrete and exterior mortar. A RC layer is coated on surface of the exterior mortar with purpose of providing passive cooling. The thickness of exterior mortar is set as 20 mm, whereas that of RC coating is neglected in this research.

Fig. 1(c) presents the two-dimensional physical model of a south wall under assumption that wall depth is infinite without producing thermal effect to width or length direction. It is found that outside surface of the south wall is subjected to solar irradiation during the daytime. The RC coating with special photothermal property enables to emit radiative power to the deep space, realizing substantial cooling effect. Meanwhile, incident atmospheric radiation can be absorbed by outside surface of the south wall. The nonradiative heat gain of RC coating from the surrounding media is capable of affecting thermal performance of the south wall. The indoor environment is assumed as an isothermal region, inducing convective heat transfer between interior of the south wall and the indoor temperature. Paraffin PCM with phase change range (17.5–22.5 °C) is selected based on consideration of the indoor design temperature. They are treated into the shape-stable material prior to be sealed in a polymer waterproof package. Thermophysical properties of building materials are included in Table 1.

2.2. Governing equations

2.2.1. Conventional building materials

Conventional building materials including mortar and concrete are always maintained in solid during the investigation. Heat transfer process of these building materials are dominated by the conduction. Contact resistance between their interfaces are ignored. The energy conservation equation can be expressed in Eq. (1).

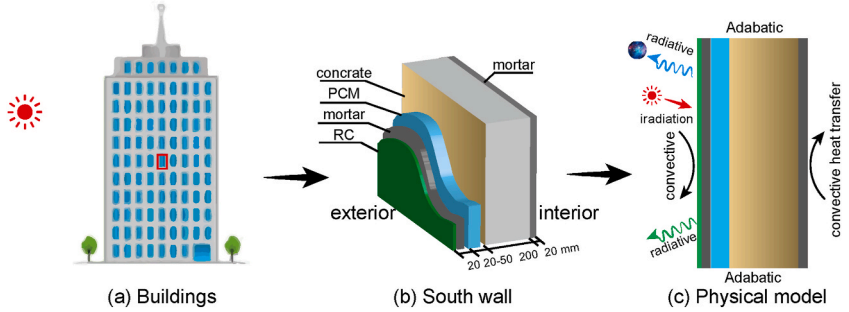

Fig. 1. Structural schematics of the studied building, south wall and related physical model.

Table 1
Thermophysical properties of building materials.

Thermophysical properties	Mortar	Brick	PCM
Density (kg/m^3)	1922	2000	860(s)/820(l)
Thermal conductivity (W/(m·°C))	1.12	0.5	0.27(s)/0.20(l)
Specific heat (J/(kg·°C))	837.4	900	1850(s)/2050(l)
Melting point (°C)	–	–	22.5(s)/17.5(l)
Latent heat (J/kg)			176000

$$\frac{\rho_p C_{p,p}\partial T}{\partial \tau} = \nabla\left(\lambda_p \nabla T\right) + S_p \quad \text{Eq. (1)}$$

where τ is the time; ρ_p, $C_{p,p}$ and λ_p are the density, specific heat and thermal conductivity of building materials; S_p denotes the source term in energy conservation equation.

2.2.2. PCM

Several reliable assumptions to simplify the theoretical modeling are firstly proposed. PCM is regarded as the incompressible material and its flow is neglected. Thermophysical properties of PCM are only varied between solid and liquid states. Phase transition occurs within a certain temperature range. The established enthalpy-porosity method is utilized to reflect phase change process of PCM [36,37]. The whole computational domain is termed as a porous zone with porosity of each cell characterized by liquid fraction. Based on the above assumption, the governing equation of PCM in terms of energy conservation is shown in Eq. (2).

$$\frac{\partial(\rho_m H)}{\partial \tau} = \nabla(\lambda_m \nabla T) + S_m \quad \text{Eq. (2)}$$

where τ is the time; ρ_m and λ_m are the density and thermal conductivity of PCM; S_m represents the source term in energy conservation equation, $S_m = -A_{mushy}\frac{(1-f)^2}{f^3+\varnothing}$, $A_{mushy} = 10^5$, $\varnothing = 0.001$; f is the volume fraction of liquid PCM; PCM enthalpy of H equals to the accumulation of sensible heat (h_s) and latent heat (L) and can be calculated through Eqs. (3) and (4).

$$H = h_s + fL \quad \text{Eq. (3)}$$

$$h_s = h_{ref} + \int_{T_{ref}}^{T} c_{p,m} dT \quad \text{Eq. (4)}$$

where h_{ref} and T_{ref} are the reference enthalpy and temperature; $c_{p,m}$ is specific heat of PCM. f is used to reflect the volume proportion of liquid PCM during the research. $f = 0$ or 1 represents all PCMs are in solid or liquid state. When PCM is in the mushy region, f will linearly change between 0 and 1.

$$f = \begin{Bmatrix} 0, \mathrm{T}_f < T_s \\ \dfrac{\mathrm{T}_f - T_s}{\mathrm{T}_l - T_s}, T_s < \mathrm{T}_f < T_l \\ 1, \mathrm{T}_f > T_l \end{Bmatrix} \quad \text{Eq. (5)}$$

where T_s and T_l are the initial and terminal temperatures of PCM melting zone.

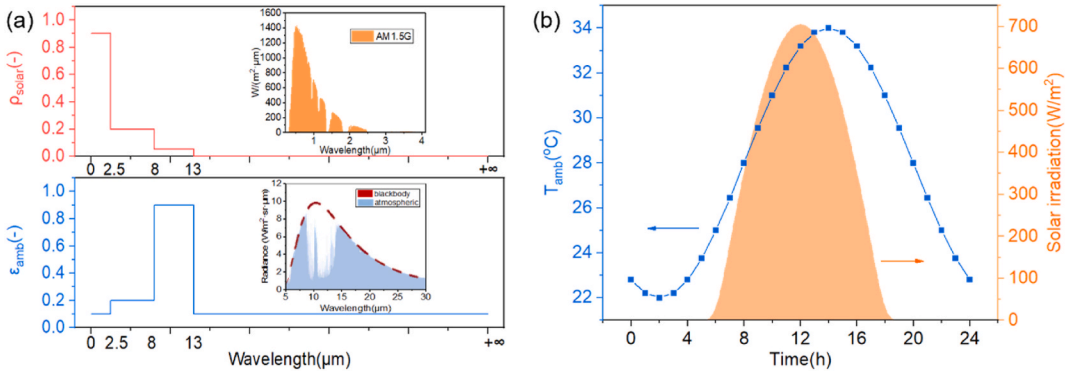

Fig. 2. Spectral characteristic of RC coating and ambient temperature.

2.2.3. RC coating

RC cooling is derived through surface-surface radiation between the exterior and ambient, as well as between the exterior and sky, as shown in Eqs. (6)–(8). A superior RC coating should have excellent reflection in solar wavelength range and radiation in atmospheric window wavelength range. The RC coating is termed as an opaque surface in the numerical analysis based on the experimental results [33]. Fig. 2 plots the detailed spectral characteristic of RC coating and it is found that excellent reflection is established through reflectivity of 0.9 in the solar wavelength range (0–2.5 μm). Meanwhile, the reflectivity of 0.2, 0.05 and 0 is adopted to the wavelength range of 2.5–8, 8–13 and 13-∞ μm, respectively. When it comes to radiation of RC coating, Table 2 and Fig. 2 display that the better radiation is accomplished by means of utilizing larger emissivity of 0.9 in atmospheric window range of 8–13 μm, leading to reduction of indoor temperature. The RC coating is designed to has emissivity of 0.1, 0.2 and 0.1 with regard to wavelength range of 0–2.5, 2.5–8 and 13-∞ μm.

$$\dot{q}_{rt} = \dot{q}_{rad} + \dot{q}_{atm} - \dot{q}_{solar} - \dot{q}_{nonrad} \quad \text{Eq. (6)}$$

$$\dot{q}_{rad} = \int cos\ \theta d\Omega \int_0^{\infty} I_{bb}(\lambda, T_m)\varepsilon_m(\Omega, \lambda)d\lambda \quad \text{Eq. (7)}$$

$$\dot{q}_{atm} = \int cos\ \theta d\Omega \int_0^{\infty} I_{bb}(\lambda, T_{atm})\varepsilon_m(\Omega, \lambda)\varepsilon_{atm}(\Omega, \lambda)d\lambda \quad \text{Eq. (8)}$$

where, ε_m is the emissivity of a radiation layer as a function of direction and wavelength; I_{bb} is the spectral radiance of blackbody; T_{atm} is the ambient temperature; ε_{atm} is the atmospheric emissivity; λ is wavelength; $\dot{q}_{solar}$ is the absorbed solar irradiation, $\dot{q}_{solar} = \alpha_m I_{solar}$; $\dot{q}_{nonrad}$ is the non-radiative heat transfer (conduction and convection) with environment.

2.3. Initial and boundary conditions

The numerical simulation is started at 0:00 with the wall initial temperature of 26 °C. The indoor temperature is maintained as constant of 26 °C in the temperature field during the study. Given that difference between indoor temperature and interior temperature exists, convective heat transfer is considered with the heat transfer coefficient of 5.7 W/($m^{2.}$°C) [8,19]. The exterior wall is contacted with solar radiation directly. Solar irradiance is fitted into a cosine function with time as shown in Fig. 2(b). It is perceived that solar irradiation is considered only at daytime (6:00–18:00). The peak power is largely dependent to the investigated date. Both convective and radiative heat transfer simultaneously happen between exterior walls and ambient with a non-radiative heat transfer coefficient of 20 W/($m^{2.}$°C) [39]. In order to simple the numerical calculation, variation of ambient temperature is supposed to follow the cosine function with time and the minimal and maximal temperatures occur at 2:00 and 14:00, respectively. There exists substantial discrepancy in terms of the maximum temperature time point and the solar peak power time point, as results of thermal inertness of the wall [18,19]. The radiative cooling is treated as a boundary condition to couple into in the energy conservation equation.

2.4. Model solving and validation

2.4.1. Model solving

The finite element method is utilized to solve the governing equations. Considering the heat transfer and solar irradiation are coupled together, COMSOL Multiphysics with the built-in finite element analysis is adopted in this study. It is recognized as an excellent tool to deal with coupling of several physical processes. The computational region is meshed into numerous structured rectangular grids. Energy conservation equations are discretized within the computational region. A backward differentiation formula (BDF) with a feasible time step is adopted and the maximum BDF order is limited to 2. The parallel direct sparse solver (PARDISO) is about to solve the residual equation. A rational error control is set to ensure reliable convergence of the model solving. In order to maintain a highly accurate resolution, relative tolerance of 10^{-5} with regard to energy conservation equation will be checked at each time step of the numerical calculation.

2.4.2. Mesh independence

Since COMSOL adopts a free BDF time step, it frequently varies between 1 and 10 during the calculation process for capturing accurate and fast results. This study would like to analyze the mesh independence rather than time step independence. It is revealed in Fig. 3(a) that four mesh numbers (17500, 31730, 45800 and 70000) are considered in the mesh independence analysis. Calculated exterior temperature and liquid fraction are discovered to be sensitive to the mesh number. When the mesh number is larger than 45800, the exterior temperature and liquid fraction present neglectable variation with augment of the mesh number. This sight indicates that the model solving based on the finite element method is independent on the mesh number under this scenario. Continuing

Table 2
Specific spectral characteristics of RC coating as function of wavelength.

Wavelength (μm)	Reflectivity(ρ_{solar})	Emissivity(ε_{amb})
0–2.5	0.9	0.1
2.5–8	0.2	0.2
8–13	0.05	0.9
13-∞	0	0.1

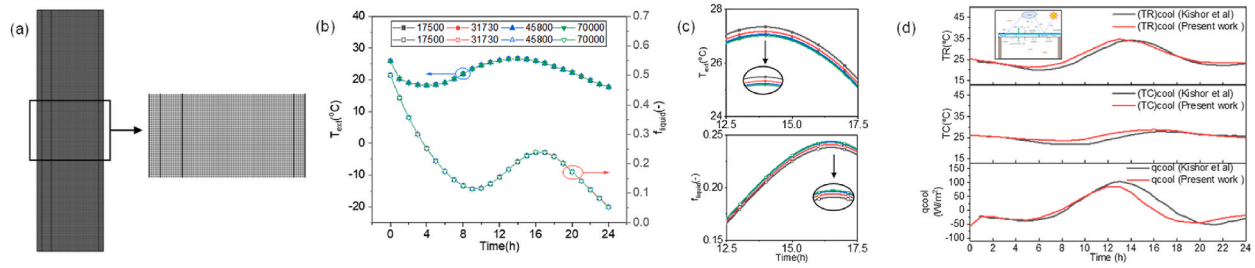

Fig. 3. Mesh independence and verification of the built numerical model. (a)Mesh structure (45800), (b)Mesh independence (0–24 h), (c)Mesh independence (12.5–17.5 h) and (d) Model verification.

to enlarge the mesh number will cause the calculated process to take amounts of time (Fig. 3(b)–(c)). Therefore, it is rationally supposed that the mesh number of 45800 is recommended in the following study based on dual considerations of computational accuracy and saving costs.

2.4.3. Model validation

In order to verify the built mathematical model, this study compares obtained results based on this numerical model with literature results in Kishor work [39]. The opaque roof (90 m^2) of a building is covered with a cool coating having its top surface exposed to solar irradiation. Solar reflectance and radiative emittance of the cool coating are 0.74 and 0.90, respectively. Sunrise and sunset occurred at 07:00 and 19:00 h with the peak hourly solar irradiation (940 W/m^2) appeared at 13:00 h. Fig. 3(d) illustrates the hourly roof temperature, ceiling temperature and conduction heat flux. It is found that simulated temperatures and heat flux agree well with the literature results, suggesting that the built numerical model is reliable. The absolute errors are respectively determined as 3.01 °C, 3.28 °C, and 16.15 W/m^2 in terms of peak roof temperature, ceiling temperature and conduction heat flux, with corresponding relative errors of 13.12 %, 12.45 % and 17.53 %. Difference between the real object and assumed physical model towards indoor thermal space might attribute to slight discrepancy between calculated and experimental results. It is inferred that the built model is accurate enough to be utilized in the following research.

3. Results and discussion

3.1. PCM addition

This study firstly analyzes thermal performance of three built walls that are separately denoted as nP-nRC (no PCM + no RC coating), nP-RC (no PCM + RC coating) and P-RC (PCM + RC coating). It is found in Fig. 4(a) that exterior temperature of the nP-nRC wall without PCM or RC coating has greater fluctuation magnitude than ambient temperature as the time elapses. Solar radiation is absorbed on the exterior wall at the daytime, leading to the exterior temperature exceeding the ambient temperature. On the contrary, the nP-nRC wall shows radiation to the environment and sky at nighttime which causes the exterior temperature lower than the ambient temperature. As for the built novel walls (P-RC and nP-RC cases), Fig. 4(a) illustrates that the RC coating is able to exert noticeable effect on the wall thermal performance, leading to the exterior temperature below the ambient temperature over the 24 h. Owing to the heat storage capacity of PCM, the P-RC wall loading PCM and RC coating reveals lighter fluctuation in terms of exterior temperature, compared to those of other walls.

Fig. 4(b) plots transient interior temperature variation of three novel walls and it is obtained that the interior temperature is largely affected by the introduction of RC coating or PCM. The nP-nRC wall is found to have fluctuating interior temperature as result of the dynamic ambient temperature. The minimum and maximum results are 25.33 °C at 10:00 and 27.64 °C at 22:00. When RC coating is employed into the wall, interior temperature of the nP-RC wall is always lower than 26 °C, owing to the continuous radiative cooling. It firstly drops to 24.73 °C at 13:00 and then climbs to 25.4 °C at 22:00. Fig. 4(b) presents that PCM enables to shift the temperature peak, ensuring the interior temperature tightly close to target temperature of 26 °C.

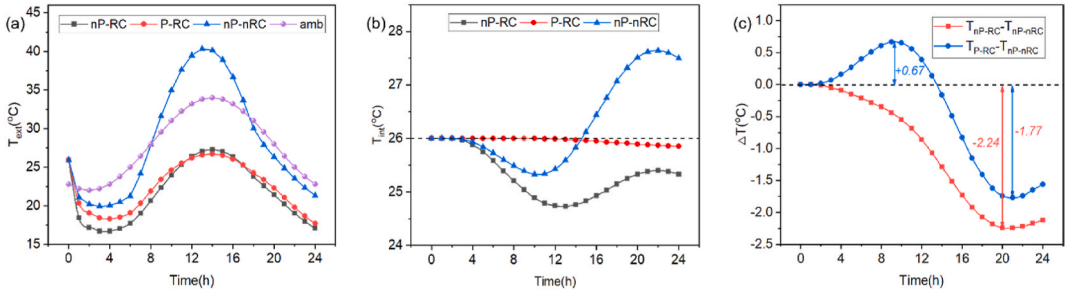

Fig. 4. Thermal performance of the built wall with and without PCM addition (PCM in outside, δ_{PCM} = 40 mm, D_{max} = 713 W/m^2, $T_{amb,ave}$ = 26 °C, T_{ind} = 26 °C). (a) Exterior temperature, (b) Interior temperature and (c) Temperature difference.

The differences between interior temperatures of two novel walls and the conventional wall are compared in Fig. 4(c). It is demonstrated that temperature difference between interior temperature of the nP-RC wall and nP-nRC wall decreases sharply with the elapse of time and arrives lowest result of −2.24 °C at 20:00. Considering thermal buffering effect of PCM, the temperature difference between interior temperatures of the P-RC wall and nP-nRC wall has remarkable fluctuation over time, firstly climbing to 0.67 °C at 9:00 and then dropping to merely −1.77 °C at 21:00. PCM is capable of reducing temperature difference fluctuation, which limits the interior temperature to slightly vary near the target temperature. Therefore, it is summarized that thermal performance of walls can be well regulated by the RC coating. PCM has the capacity of improving effect of RC coating on thermal performance of the walls.

3.2. PCM location

Thermal performance of built P-RC walls as function of PCM location is indicated in Fig. 5. It is discovered that RC coating produces remarkable radiative cooling to the multilayer wall, which leads to the exterior temperature lower than the ambient temperature (20–32 °C). Since PCM stores or releases thermal energy under approximately isothermal condition, it enables to buffer the exterior temperature, inducing lower peak and higher valley in terms of the exterior temperature as shown in Fig. 5(b). PCM located closer to the exterior wall has more obvious buffer effect on the exterior temperature. It is specific that the valley temperature of exterior wall is 18.31 °C when PCM is installed on outside of the wall, decreasing with the PCM location away from the exterior wall, and declines to 16.73 °C for the inside PCM case. The peak temperature of exterior wall with PCM located in outside is merely 26.71 °C, which is lower than exterior walls containing PCM in middle and inside locations.

The interior temperature initially maintains constant and then decreases slightly with the augment of time. The interior temperature drops from 26 to 25.94 °C when PCM is placed inside of the wall. Stored thermal energy in PCM will release later on inside of the multilayer wall, resulting in stronger buffer effect to interior temperature. This well corresponds to less interior temperature decline in Fig. 5(c). The multilayer walls with PCM in middle and outside are found to have interior temperature as low as 25.93 and 25.85 °C. Obtained results confirm that interior temperature is insensitive to PCM location.

Regarding that PCM will experience switching between melting and solidification, the PCM liquid fraction fluctuates substantially as time elapses. Outside PCM melts rapidly to release thermal energy to compensate the heat dissipation of radiative cooling, displaying lowest liquid fraction in Fig. 5(d). As PCM moves from outside to inside of the multilayer wall, radiative cooling effect of RC coating on the wall is attenuated, revealing higher PCM liquid fraction in comparison to outside case. It is specific that PCM liquid fraction of the multilayer wall with PCM arranged on outside is 0.0534 at 24 h, separately increasing to 0.3376 and 0.4223 in the multilayer walls with PCM on middle and inside locations.

3.3. PCM thickness

Fig. 6 plots thermal performance of built P-RC walls changed with the PCM thickness. It is apparent that exterior temperatures vary limited with growth of PCM thickness, only indicating light enlargement at the low temperature time periods (4:00–9:00 and 20:00–24:00). The exterior temperature can individually drop down to 17.07, 17.35, 17.72 and 17.82 °C in the PCM thickness of 20, 30, 40 and 50 mm. Obtained results prove that exterior temperature of walls is primarily influenced by ambient temperature.

Fig. 6(b) shows that interior temperatures of walls fluctuate sharply with augment of the PCM thickness. As the PCM thickness rises, the interior temperatures increase over the studied time period, owing to effective thermal inertness of walls enhanced by PCM. Effect of ambient temperature variation on the interior temperature can be weakened. The interior temperatures reduce steadily as time elapses when the PCM thickness exceeds 30 mm. The minimal result is determined as 25.43 °C in built wall with PCM thickness of 20 mm. The walls present minimal interior temperatures of 25.7, 25.85 and 25.94 °C in walls containing PCM thickness of 30–50 mm, respectively. Thermal buffering of PCM also contributes to the time lag to the interior valley temperature. Thicker PCM results in larger time lag to the interior temperature.

Liquid fraction of PCM varied with PCM thickness is depicted in Fig. 6(c). PCM solidifies to release thermal energy to maintain interior temperature within target of 26 °C. It is detected that PCM thickness is capable of substantially affecting liquid fraction of PCM. When the PCM thickness is 20 mm, liquid fraction of PCM oscillates with the elapse of time, dropping to almost 0 at time periods (5:00–10:00 and 22:00–24:00) and climbing to maximum of 0.214 at 16:00. Liquid fraction of PCM increases accordingly as the PCM thickness rises to 30–50 mm. It is specific that the minimal liquid fractions of PCM are individually 0.014, 0.115 and 0.189 for walls including PCM thickness of 30, 40 and 50 mm. Similarly, the related PCMs show maximal liquid fractions of 0.193, 0.239 and 0.281,

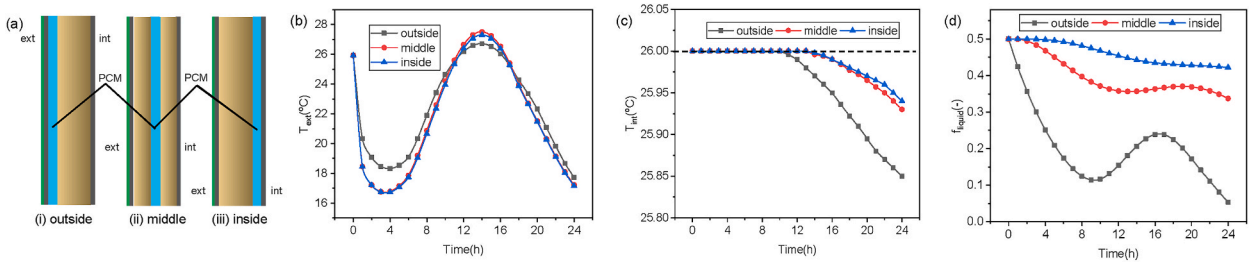

Fig. 5. Thermal performance of built P-RC walls as function of PCM location (δ_{PCM} = 40 mm, D_{max} = 713 W/m^2, $T_{amb,ave}$ = 26 °C, T_{ind} = 26 °C). (a) PCM wall structure, (b) Exterior temperature, (c) Interior temperature and (d) PCM liquid fraction.

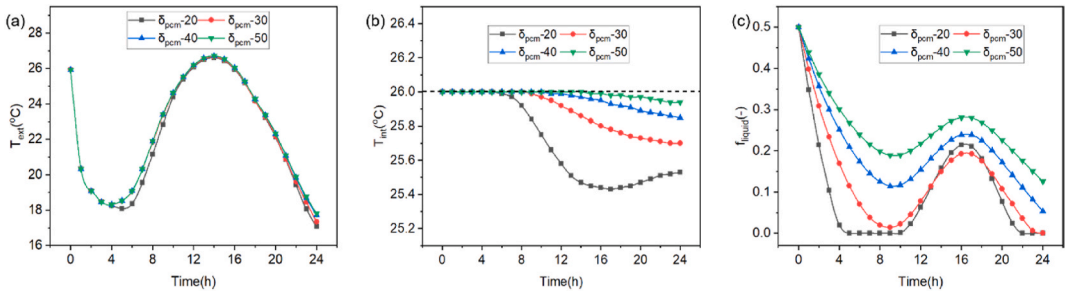

Fig. 6. Thermal performance of built P-RC walls as function of PCM thickness (PCM in outside, D_{max} = 713 W/m^2, $T_{amb,ave}$ = 26 °C, T_{ind} = 26 °C). (a) Exterior temperature, (b) Interior temperature and (c) PCM liquid fraction.

revealing that only partial PCM experiences phase transition during the investigation.

3.4. Solar radiation

Effects of solar radiation intensity on thermal performance of built P-RC walls are elaborated in Fig. 7. It is perceived that transient exterior temperatures change obviously with elapse of time, owing to the variation of solar radiation intensity and ambient temperature. When the peak of solar radiation rises from 313 to 913 W/m^2, slight growth is observed in the maximal exterior temperature, continuously increasing from 25.65 °C to 27.25 °C. This sight is attributed to improvement of thermal energy absorption under large solar radiation intensity.

Fig. 7(b) shows the interior temperature decreases with augment of solar radiation intensity. Obvious enhancement to the interior temperature is observed at solar radiation period (6:00–18:00). This is because that PCM is capable of offering thermal buffering to thermal performance of built P-RC walls. When PCM releases stored thermal energy, the interior temperature can be noticeably influenced. It can be inferred that interior temperature is hardly influenced by the solar radiation intensity under combined actions of RC coating and PCM.

Transient liquid fractions of PCMs are also illustrated in Fig. 7(c). It is obvious that liquid fractions of PCMs drop substantially in the initial stage due to the thermal energy released to indoor thermal environment. With increase of ambient temperature and solar radiation, PCM begins to absorb thermal energy and related liquid fraction rises steadily. Larger solar radiation intensity promotes the thermal energy storage rate of PCM, resulting in higher PCM liquid fraction. It is specific that maximal liquid fraction increases from 0.166 to 0.276 as the solar radiation rises from 313 to 913 W/m^2. Liquid fractions of PCMs then decrease as time elapses, accompanied by thermal energy discharging to maintain indoor comfortable temperature.

3.5. Ambient temperature

Fig. 8 indicates thermal performance of built P-RC walls as function of ambient temperature. It is obtained in Fig. 8(a) that ambient temperature has remarkable influence on exterior temperature that rises with augment of the ambient temperature. More thermal energy is absorbed on the exterior surface at higher ambient temperature, leading to the higher exterior temperature. The peak temperature is calculated to climb from 17.88 °C to 21.26, 24.41, 26.71 and 29.24 °C for average ambient temperatures of 18, 22, 26 and 30 °C, respectively.

Interior temperatures are identical to the target temperature of 26 °C in the initial no radiation period (0–8:00). The heat dissipation rate produced by the RC coating, radiative and convective heat transfer contributes to interior temperature drop slowly as the time elapses. More intense radiative and convective heat transfer happen between walls and ambient at lower ambient temperature. Larger ambient temperature is favorable to reduce the temperature difference between interior temperature and target temperature, producing higher indoor temperature. It is determined that the P-RC walls obtain highest interior temperature of 24.48–25.94 °C within the studied ambient temperature range.

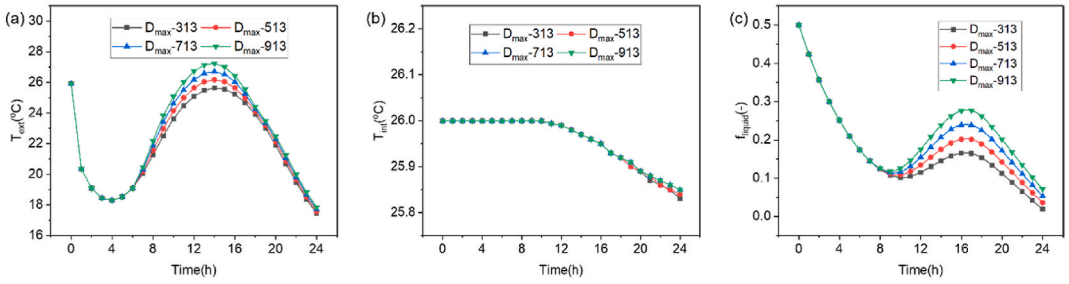

Fig. 7. Thermal performance of built P-RC walls as function of solar radiation intensity ($I_{DNI} = D_{max} \times abs\left(\cos\left(\frac{2\pi(t-12)}{24}\right)\right), 6 < t < 18h$, PCM in outside, δ_{PCM} = 40 mm, $T_{amb,ave}$ = 26 °C, T_{ind} = 26 °C). (a) Exterior temperature, (b) Interior temperature and (c) PCM liquid fraction.

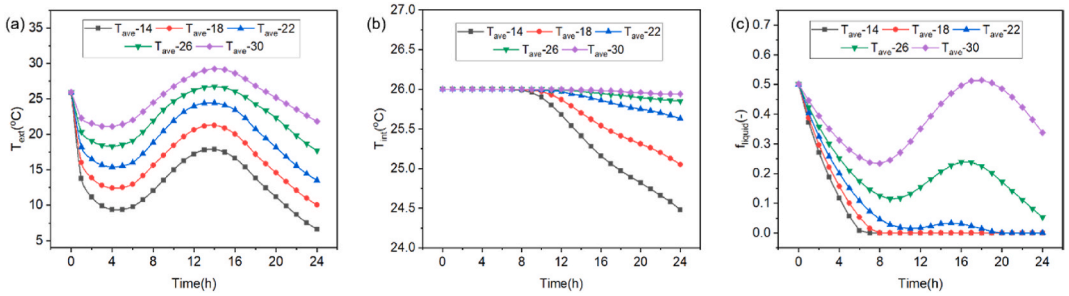

Fig. 8. Thermal performance of built P-RC walls as function of ambient temperature ($T_{amb} = T_{ave} + 6 \times \cos\left(\frac{2\pi(t-14)}{24}\right)$, PCM in outside, $\delta_{PCM} = 40$ mm, $D_{max} = 713$ W/m^2, $T_{ind} = 26$ °C). (a) Exterior temperature, (b) Interior temperature and (c) PCM liquid fraction.

The ambient temperature enables to generate fluctuation to transient liquid fraction of PCM embedded in P-RC walls, as shown in Fig. 8(c). Thermal energy charged in or discharged out of PCM is heavily affected by heat transfer between the exterior wall and ambient. It is found that liquid fraction of PCM can even decline down to 0, when the average ambient temperature is less than 22 °C. Higher ambient temperature is conducive to thermal energy accumulated in the PCM, revealing larger PCM liquid fraction. The peak liquid fractions of PCMs are individually calculated as 0.239 at 16:00 and 0.512 at 17:00 for average ambient temperatures of 26–30 °C.

3.6. Indoor temperature

Fig. 9 depicts thermal performance of built P-RC walls varied with the indoor temperature. It is seen that exterior temperature presents fluctuation similar to that of ambient temperature. Higher indoor temperature means more thermal energy transferred from indoor environment to the walls, inducing larger exterior temperature, especially in terms of valley temperatures. It is determined that exterior valley temperature of the P-RC wall is obtained as 15.27 °C and then climbs to 19.51 °C as the indoor temperature rises from 20 to 28 °C.

The interior temperature is less sensitive to indoor temperature compared to exterior temperature. It is apparent that slight fluctuations can be observed in terms of indoor temperatures. This sight is decided by the heat conduction to the exterior and convective heat transfer between interior and indoor environment. The maximal deviations between interior temperature and target temperature are found as +0.34, −0.42, −0.57, −0.15 and −0.23 °C, respectively. The wall exhibits the lowest deviation when the indoor temperature is closest to target temperature of 26 °C, which deduces that PCM with the melting point close to the indoor target temperature is recommended to be utilizes in P-RC walls.

The indoor temperature directly determines the initial PCM liquid fraction, under assumption that initial PCM temperature equals to indoor initial temperature. When the indoor temperature is below 24 °C, the related liquid fraction is less than 0.1, which means that PCM merely acts as insulation in the solid form. As the indoor temperature is larger than 26 or 28 °C, liquid fraction of PCM fluctuates with elapse of time as result of switching between heat storage and heat release. Larger indoor temperature implies more thermal energy can be stored in PCM in the form of latent heat, leading to higher liquid fraction of PCM incorporated in the P-RC walls. The peaks of PCM liquid fractions are specified as 0.239 and 0.598 for the walls at indoor temperatures of 26 and 28 °C.

4. Conclusions

PCM is introduced into the south wall of a multistory building to modify the cooling derived from a radiative cooler. A novel multilayer P-RC wall consisting of a RC layer, PCM layer, a concrete and two motors is configured to passively regulate heat gain and dissipation, maintaining indoor thermal comfortable environment. This study highlights superiority of the built P-RC wall over a conventional wall or a RC wall. Performance of the built P-RC wall changed with various parameters is also discussed.

Results indicate that the RC coating brings exterior temperature below the ambient temperature over the 24 h, achieving maximum exterior temperature drop of 13.63 °C. Heat storage capacity of PCM induces exterior temperature of the P-RC wall to have slighter fluctuation compared to the nP-RC wall. PCM enables to shave the temperature peak and shift the temperature valley, maintaining interior temperature tightly close to target temperature. Radiative cooling of RC coating on the wall is attenuated as the phase change material moves inward, resulting in PCM liquid fraction dropping from 0.4223 in outside PCM wall to 0.0534 in inside PCM wall at 24 h. Interior temperature increases with growth of PCM thickness and ambient temperature and indoor temperature. Larger PCM thickness, higher ambient temperature and indoor temperature induce the interior temperature closer to target temperature. More thermal energy is absorbed on the exterior surface at higher solar radiation intensity, leading to the higher exterior temperature and larger PCM liquid fraction. Lower indoor temperature means less thermal energy dissipated from indoor environment, resulting in less PCM liquid fraction accordingly.

In conclusion, this novel P-RC system combine the dual effects of radiative cooling and latent heat thermal energy storage, which is beneficial to offer a passive strategy to achieve building thermal control.

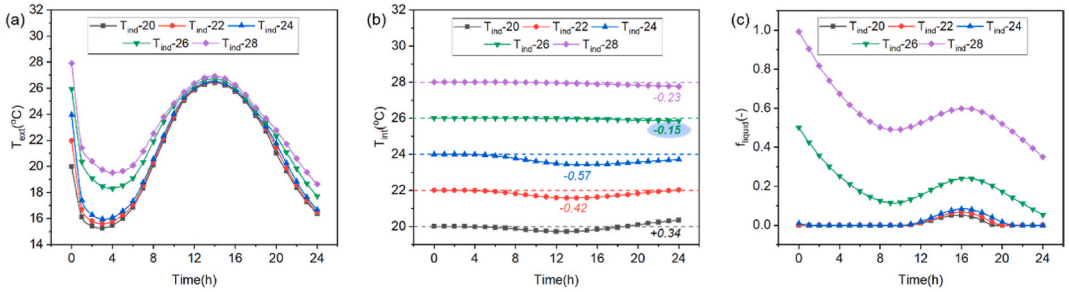

Fig. 9. Thermal performance of built P-RC walls as function of indoor temperature (PCM in outside, $\delta_{PCM} = 40$ mm, $D_{max} = 713$ W/m^2, $T_{amb,ave} = 26$ °C). (a) Exterior temperature, (b) Interior temperature and (c) PCM liquid fraction.

CRediT authorship contribution statement

Zhaoli Zhang: Conceptualization, Data curation, Writing – original draft. **Jiayu Liu:** Data curation, Formal analysis. **Nan Zhang:** Funding acquisition, Resources, Supervision. **Xiaoling Cao:** Supervision, Visualization. **Yanping Yuan:** Funding acquisition, Supervision, Visualization. **Muhammad Sultan:** Supervision, Validation. **Shady Attia:** Resources, Visualization.

Declaration of competing interest

The authors declare that they have no known competing financial interests or personal relationships that could have appeared to influence the work reported in this paper.

Data availability

Data will be made available on request.

Acknowledgements

This work was supported by the National Natural Science Foundation of China (NO. 52108077 and 52378111), Natural Science Foundation of Sichuan Province (No. 2023NSFSC0896), Natural Science Foundation of Chongqing, China (No. CSTB2022NSCQ-MSX0604).

References

[1] X. Yu, J. Chan, C. Chen, Review of radiative cooling materials: performance evaluation and design approaches, Nano Energy 88 (2021), 106259.
[2] Z. Li, Q. Chen, Y. Song, B. Zhu, J. Zhu, Fundamentals, materials, and applications for daytime radiative cooling, Adv. Mater. Technol. 5 (2020), 1901007.
[3] L. Rincón, A. Carrobé, I. Martorell, M. Medrano, Improving thermal comfort of earthen dwellings in sub-Saharan Africa with passive design, J. Build. Eng. 24 (2019), 100732.
[4] C. Dias, R.C. Veloso, J. Maia, N.M.M. Ramos, J. Ventura, Oversight of radiative properties of coatings pigmented with TiO2 nanoparticles, Energy Build. 271 (2022), 112296.
[5] P. Srivastava, Y. Khan, M. Bhandari, J. Mathur, R. Pratap, Calibrated simulation analysis for integration of evaporative cooling and radiant cooling system for different Indian climatic zones, J. Build. Eng. 19 (2018) 561–572.
[6] D. Li, X. Liu, W. Li, Z. Lin, B. Zhu, Z. Li, J. Li, B. Li, S. Fan, J. Xie, Scalable and hierarchically designed polymer film as a selective thermal emitter for high-performance all-day radiative cooling, Nat. Nanotechnol. 16 (2021) 153–158.
[7] J. Liu, Z. Zhou, J. Zhang, W. Feng, J. Zuo, Advances and challenges in commercializing radiative cooling, Mater. Today Phys. 11 (2019), 100161.
[8] J. Yuan, H. Yin, D. Yuan, Y. Yang, S. Xu, On daytime radiative cooling using spectrally selective metamaterial based building envelopes, Energy 242 (2022), 122779.
[9] A. Pirvaram, N. Talebzadeh, S.N. Leung, P.G. O'Brien, Radiative cooling for buildings: a review of techno-enviro-economics and life-cycle assessment methods, Renew. Sustain. Energy Rev. 162 (2022), 112415.
[10] J. Song, W. Zhang, Z. Sun, M. Pan, F. Tian, X. Li, M. Ye, X. Deng, Durable radiative cooling against environmental aging, Nat. Commun. 13 (2022) 4805.
[11] M.-C. Huang, C.-H. Xue, J. Huang, B.-Y. Liu, X.-J. Guo, Z.-X. Bai, R.-X. Wei, H.-D. Wang, M.-M. Du, S.-T. Jia, A hierarchically structured self-cleaning energy-free polymer film for daytime radiative cooling, Chem. Eng. J. 442 (2022), 136239.
[12] Y. Dong, H. Han, F. Wang, Y. Zhang, Z. Cheng, X. Shi, Y. Yan, A low-cost sustainable coating: improving passive daytime radiative cooling performance using the spectral band complementarity method, Renew. Energy 192 (2022) 606–616.
[13] X. Hu, Y. Zhang, J. Zhang, H. Yang, F. Wang, B. Fei, N. Noor, Sonochemically-coated transparent wood with ZnO: passive radiative cooling materials for energy saving applications, Renew. Energy 193 (2022) 398–406.
[14] J. Khedari, J. Waewsak, S. Thepa, J. Hirunlabh, Field investigation of night radiation cooling under tropical climate, Renew. Energy 20 (2000) 183–193.
[15] M.G. Meir, J.B. Rekstad, O.M. Løvvik, A study of a polymer-based radiative cooling system, Sol. Energy 73 (2002) 403–417.
[16] G. Heidarinejad, M. Farmahini Farahani, S. Delfani, Investigation of a hybrid system of nocturnal radiative cooling and direct evaporative cooling, Build. Environ. 45 (2010) 1521–1528.
[17] S. Zhang, J. Niu, Cooling performance of nocturnal radiative cooling combined with microencapsulated phase change material (MPCM) slurry storage, Energy Build. 54 (2012) 122–130.
[18] C.Y. Tso, K.C. Chan, C.Y.H. Chao, A field investigation of passive radiative cooling under Hong Kong's climate, Renew. Energy 106 (2017) 52–61.
[19] M. Sameti, A. Kasaeian, Numerical simulation of combined solar passive heating and radiative cooling for a building, Build. Simul. 8 (2015) 239–253.
[20] M.H.A. Nasir, A.S. Hassan, Thermal performance of double brick wall construction on the building envelope of high-rise hotel in Malaysia, J. Build. Eng. 31 (2020), 101389.

[21] S. Mohamed, H. Al-Khatri, J. Calautit, S. Omer, S. Riffat, The impact of a passive wall combining natural ventilation and evaporative cooling on schools' thermal conditions in a hot climate, J. Build. Eng. 44 (2021), 102624.
[22] E. Katramiz, N. Ghaddar, K. Ghali, Daytime radiative cooling: to what extent it enhances office cooling system performance in comparison to night cooling in semi-arid climate? J. Build. Eng. 28 (2020), 101020.
[23] A. Zaite, N. Belouaggadia, C. Abid, M. Ezzine, Performance improvement of photovoltaic cells using night radiative cooling technology in a PV/T collector, J. Build. Eng. 42 (2021), 102843.
[24] N. Wang, Y. Lv, D. Zhao, W. Zhao, J. Xu, R. Yang, Performance evaluation of radiative cooling for commercial-scale warehouse, Mater. Today Energy 24 (2022), 100927.
[25] Z. Cheng, H. Han, F. Wang, Y. Yan, X. Shi, H. Liang, X. Zhang, Y. Shuai, Efficient radiative cooling coating with biomimetic human skin wrinkle structure, Nano Energy 89 (2021), 106377.
[26] Z. Yi, D. Xu, J. Xu, H. Qian, D. Zhao, R. Yang, Energy saving analysis of a transparent radiative cooling film for buildings with roof glazing, Energy Built Environ 2 (2021) 214–222.
[27] K. Zhou, N. Miljkovic, L. Cai, Performance analysis on system-level integration and operation of daytime radiative cooling technology for air-conditioning in buildings, Energy Build. 235 (2021), 110749.
[28] J. Anand, D.J. Sailor, A. Baniassadi, The relative role of solar reflectance and thermal emittance for passive daytime radiative cooling technologies applied to rooftops, Sustain. Cities Soc. 65 (2021), 102612.
[29] S. Yoon, M. Kim, J. Seo, S. Kim, H. Lee, J. Lee, B.J. Lee, Performance analysis of a hybrid HVAC system consisting of a solar thermal collector and a radiative cooling panel, Energy Build. 241 (2021), 110921.
[30] K. Lin, L. Chao, T.C. Ho, C. Lin, S. Chen, Y. Du, B. Huang, C.Y. Tso, A flexible and scalable solution for daytime passive radiative cooling using polymer sheets, Energy Build. 252 (2021), 111400.
[31] K. Tang, K. Dong, J. Li, M.P. Gordon, F.G. Reichertz, H. Kim, Y. Rho, Q. Wang, C.Y. Lin, C.P. Grigoropoulos, A. Javey, J.J. Urban, J. Yao, R. Levinson, J. Wu, Temperature-adaptive radiative coating for all-season household thermal regulation, Science 374 (2021) 1504–1509, 80-.
[32] P. Yang, J. He, Y. Ju, Q. Zhang, Y. Wu, Z. Xia, L. Chen, S. Tang, Dual-mode integrated janus films with highly efficient NaH2PO2-enhanced infrared radiative cooling and solar heating for year-round thermal management, Adv. Sci. 2206176 (2023) 1–10.
[33] Y. Cui, X. Luo, F. Zhang, L. Sun, N. Jin, W. Yang, Progress of passive daytime radiative cooling technologies towards commercial applications, Particuology 67 (2022) 57–67.
[34] X. Kong, L. Wang, H. Li, G. Yuan, C. Yao, Experimental study on a novel hybrid system of active composite PCM wall and solar thermal system for clean heating supply in winter, Sol. Energy 195 (2020) 259–270.
[35] W. He, C. Yu, J. Yang, B. Yu, Z. Hu, D. Shen, X. Liu, M. Qin, H. Chen, Experimental study on the performance of a novel RC-PCM-wall, Energy Build. 199 (2019) 297–310.
[36] E. Tunçbilek, M. Arıcı, M. Krajčík, S. Nižetić, H. Karabay, Thermal performance based optimization of an office wall containing PCM under intermittent cooling operation, Appl. Therm. Eng. 179 (2020), 115750.
[37] T. Yan, J. Li, J. Gao, X. Xu, J. Yu, Model validation and application of the coupled system of pipe-encapsulated PCM wall and nocturnal sky radiator, Appl. Therm. Eng. 194 (2021), 117057.
[38] J.C. Kurnia, L.A.F. Haryoko, I. Taufiqurrahman, L. Chen, L. Jiang, A.P. Sasmito, Optimization of an innovative hybrid thermal energy storage with phase change material (PCM) wall insulator utilizing Taguchi method, J. Energy Storage 49 (2022), 104067.
[39] K.T. Zingre, M.P. Wan, S. Tong, H. Li, V.W.-C. Chang, S.K. Wong, W.B. Thian Toh, I.Y. Leng Lee, Modeling of cool roof heat transfer in tropical climate, Renew. Energy 75 (2015) 210–223.